http://link.springer.com/article/10.1007/s10652-005-0243-7#page-2

Environmental Fluid Mechanics (2005) 5: 135–167 © Springer 2005

Monitoring the Transport of Biomass Burning Emissions in South America

SAULO R. FREITAS[a,*], KARLA M. LONGO[a], MARIA A.F. SILVA DIAS[b], PEDRO L. SILVA DIAS[b], ROBERT CHATFIELD[c], ELAINE PRINS[d], PAULO ARTAXO[b], GEORG A. GRELL[e] and FERNANDO S. RECUERO[b]
[a]*Center for Weather Prediction and Climate Studies - CPTEC/INPE, Brazil;* [b]*University of São Paulo, Brazil;* [c]*NASA Ames Research Center, U.S.A.;* [d]*NOAA/NESDIS/ORA, Madison, WI, U.S.A.;* [e]*Cooperative Institute for Research in Environmental Science (CFRES), University at Colorado, and NOAA Research – Forecast Systems Laboratory, Boulder, CO, U.S.A.*

Received 16 June 2003; accepted in revised form 3 May 2004

Abstract. The atmospheric transport of biomass burning emissions in the South American and African continents is being monitored annually using a numerical simulation of air mass motions; we use a tracer transport capability developed within RAMS (Regional Atmospheric Modeling System) coupled to an emission model. Mass conservation equations are solved for carbon monoxide (CO) and particulate material (PM2.5). Source emissions of trace gases and particles associated with biomass burning activities in tropical forest, savanna and pasture have been parameterized and introduced into the model. The sources are distributed spatially and temporally and assimilated daily using the biomass burning locations detected by remote sensing. Advection effects (at grid scale) and turbulent transport (at sub-grid scale) are provided by the RAMS parameterizations. A subgrid transport parameterization associated with moist deep and shallow convection, not explicitly resolved by the model due to its low spatial resolution, has also been introduced. Sinks associated with the process of wet and dry removal of aerosol particles and chemical transformation of gases are parameterized and introduced in the mass conservation equation. An operational system has been implemented which produces daily 48-h numerical simulations (including 24-h forecasts) of CO and PM2.5, in addition to traditional meteorological fields. The good prediction skills of the model are demonstrated by comparisons with time series of PM2.5 measured at the surface.

Key words: aerosol transport, air pollution, atmospheric modeling, biomass burning, climate change, long-distance transport, weather forecast

1. Introduction

The high concentration of aerosol particles and trace gases observed in the Amazon and Central Brazilian atmosphere during the dry season is associated with intense anthropogenic biomass burning activity (vegetation fires). A widely cited estimate

*Corresponding author, E-mail: sfreitas@cptec.inpe.br

suggests that biomass burning in South America is responsible for the emission of 30 Tg year^{-1} of aerosol particles to the atmosphere [1]. Most of the particles are in the fine particle fraction of the size distribution, which can remain in the atmosphere for approximately a week [2]. Estimates of biomass burning emissions as high as these are disputed by those making detailed studies of subtropical landscapes [3], and are thought to vary widely from year to year [4]. Consequently, annual monitoring is an important effort. In addition to aerosol particles, biomass burning produces water vapor and carbon dioxide, and is a major source of other compounds such as carbon monoxide (CO), volatile organic compounds, nitrogen oxides ($NO_x = NO + NO_2$), and organic halogen compounds. In the presence of abundant solar radiation and high concentrations of NO_x, the oxidation of CO and hydrocarbons is followed by ozone (O_3) formation.

In GOES-8 visible imagery Prins *et al.* [5] have observed immense regional smoke plumes in South America covering an area of approximately 4 to 5 million km^2 during the biomass-burning season. Inhalable aerosol particles ($d_p < 10\ \mu m$) with concentrations as high as 400 μg m^{-3} have been measured near the surface level and the vertically integrated smoke aerosol optical thickness column rises as high as 4.0 (440 nm) in Central Brazil [6–8]. The biomass burning particles, made up primarily of partially oxidized organic matter mixed with black-carbon, are highly efficient scatterers and absorbers of solar radiation; a single scattering albedo as low as 0.82 has been estimated for these particles [9].

On a regional and global scale, a persistent and heavy smoke layer over an extensive tropical region may alter the radiation balance and hydrologic cycling. Modeling efforts of Jacobson [10] and Sato *et al.* [11] have suggested that black-carbon radiative forcing could balance the cooling effects of the global anthropogenic sulfate emissions. The direct global radiative forcing of black-carbon is estimated to be 0.55 Wm^{-2}, corresponding to 1/3 of the CO_2 forcing. In terms of direct radiative forcing, this would elevate black-carbon to one of the most important elements in global warming, second only to CO_2 [12].

The presence of biomass burning particles in the atmosphere may also modify the solar radiative balance by changing cloud microphysics. These particles act as cloud condensation and ice nuclei, promoting changes in the cloud drops spectrum and so altering the cloud albedo and precipitation [13, 14]. This suggests that biomass burning effects may extrapolate from the local scale and be determinant in the pattern of planetary redistribution of energy from the tropics to medium and high latitudes via convective transport processes.

Several atmospheric pollutant transport models on regional or global scales have been used. Grell *et al.* [15] describe a multiscale complex chemistry model coupled to the Penn State/NCAR nonhydrostatic mesoscale model (MM5). Chatfield *et al.* [16] use the Global-Regional Atmospheric Chemistry Event Simulator (GRACES) to introduce a conceptual model of how fire emissions and chemistry produce the African/Oceanic plumes. Chatfield *et al.* [17] present a connection between tropical emissions and an observed subtropical plume of carbon monoxide at remote

areas over the Pacific Ocean, using the GRACES and MM5 models. The Georgia Tech/Goddard Global Ozone Chemistry Aerosol Radiation and Transport (GOCART) model is an example of a global transport model. Chin *et al.* [18] employed GOCART to simulate the atmospheric global sulfur cycle. MOZART (Model of Ozone And Related Tracers) is another "off-line" global chemical transport model appropriate for simulating the three-dimensional distribution of chemical species in the atmosphere [19, 20]. The term 'off-line' indicates the transport model is driven using outputs from an atmospheric model previously run or by atmospheric analysis data assimilation. 'On-line' transport models have considerable benefits since they can use the same temporal and spatial resolution of the atmospheric model, avoiding errors associated to numerical interpolation. More significantly, they are suitable for feedback studies between the tracers and the atmosphere (e.g. the effects of aerosol on the radiative transfer).

In this paper a tracer transport model coupled to the Regional Atmospheric Modeling System – RAMS [21] will be described. The tracer transport simulation is made simultaneously, or 'on-line', with the atmospheric state evolution. As a result, a real time monitoring transport system has been implemented using the coupled transport-atmospheric model. This operational system was designed to forecast and study the transport of biomass burning aerosol and gaseous species in the South American and African continents with an application during to the 2002 dry season.

The specification of the biomass burning description and the source emission parameterization will be described in Section 2. The coupled transport-atmospheric model will be presented in Sections 3 and 4. Results described in the context of our description of the transport of aerosol and gases as well as some comparisons with observations are shown in Section 4. Conclusions and recommendations are presented in Section 5.

2. Overview of Biomass Burning Emissions and Transport in South America

The ignition, evolution and behavior of a biomass fire and its emissions depend on many factors which are ultimately controlled by the environment. Local climate is extremely important in the determination of the amount and characteristics of the biomass available. For a given type of biomass, the local weather, including temperature, precipitation, humidity and wind, controls the conditions required for the fire ignition and maintenance.

Biomass burning can be described in four basic stages: ignition, flaming, smoldering and extinction [22]. The flaming stage is a pyrolitic process, with elevated temperatures as high as 1800 K, that acts to break apart the biomass molecules and decompose compounds of high molecular weight mostly into lower molecular-weight species, but also producing soot and tar along with the principle product. Nitrogen oxides, hydrocarbons and an abundance of aerosol particles are also emitted during the flaming stage. CO and other compounds characterized by incomplete

oxidation as well as aerosol particles are emitted primarily during the smoldering phase at temperatures typically below 1000 K [23]. The amount of water in the biomass is one of the most important biomass burning control factors and can determine which stage, flaming or smoldering, will be more significant and defines the ratio between the emitted CO and CO_2.

Ward *et al.* [23] estimated the amount of biomass over the ground for savanna (campo Limpo, campo Sujo, campo cerrado and cerrado *stricto sensu*) and primary and secondary-growth tropical forests, ranging from 0.71 to 29.24 kg m^{-2}. The associated standard errors ranged between 0.05 to 0.08 kg m^{-2} for the savanna classes and 1.68 to 3.58 kg m^{-2} for the primary and second-growth forests, respectively. The combustion factors (percentile of biomass effectively burned) ranged from 52 to 100%, depending on the vegetation type and the phase of combustion and showed standard errors ranging between 0 and 8.2% for the savanna classes and from 2.93 and 3.61% for the primary and second-growth forests, respectively. The higher values for the amount of biomass and lower values for combustion factor were observed for the forest sites.

The emission factor gives the total amount of generic compound emitted in terms of the total biomass consumed. Ward *et al.* [23] estimate that a cerrado fire emits on average 1700 g[CO_2]/kg[biomass burned] and 60 g[CO]/kg[biomass burned], while for the forest sites the emission factors were on average 1600 and 125 g/kg for the CO_2 and CO, respectively. In the cerrado fuel biomass is primarily consumed during the flaming phase. However, in forested sites the fraction of fuel consumed during the flaming and smoldering phases was observed to be approximately equal. These results are comparable with the estimates of Ferek *et al.* [24], based on aircraft measurements conducted during the SCAR-B (Smoke, Clouds and Radiation-Brazil, 1995) field campaign. Average values of CO_2 and CO emission factors of 1700 and 66.5 g/kg were reported for the cerrado areas, respectively. For forest areas, during the flaming phase, emission factors of 1670 and 70 g/kg were estimated for CO_2 and CO, respectively, contrasting with 1524 and 140 g/kg for the smoldering phase. Andreae and Merlet [25] compiled emission factors from the literature and produced estimates for several species. For CO the numbers were 65 ± 20 g/kg for savanna and grassland and 104 ± 20 g/kg for tropical forest. PM2.5 ranged from 5.4 ± 1.5 g/kg for savanna and grassland and 9.1 ± 1.5 g/kg for tropical forest.

Based on the estimated values of the amount of biomass over the ground (α), the combustion factor (β) and the emission factor (EF), it is possible to estimate the quantity emitted of a certain species [η] during a burning event if the burning area (a_{fire}) and the type of vegetation can be determined. This can be accomplished using the following equation.

$$M^{[\eta]} = \alpha_{\text{veg}} \cdot \beta_{\text{veg}} \cdot EF^{[\eta]}_{\text{veg}} \cdot a_{\text{fire}}. \tag{1}$$

Here the unit for $M^{[\eta]}$ is kg. For use in the model, we have selected the following set of parameters described in Table I.

Table I. Values actually used in the model for some parameters in Equation (1).

Biome category	Emission factor for CO (g/kg)	Emission factor for PM2.5 (g/kg)	Aboveground biomass density (α, kg/m^2)	Combustion factor (β, fraction)
Tropical forest[1]	110.	8.3	20.7	0.48
South America savanna[2]	63.	4.4	0.9	0.78
Pasture[3]	49.	2.1	0.7	1.00

Average values for primary and second-growth tropical forests, [2]Average values for campo cerrado (C3) and cerrado sensu stricto (C4), [3]value for campo limpo (C1). All numbers are from Ward *et al.* [23].

The large spatial extent of occurrence of biomass burning over South America makes remote sensing the only feasible way of monitoring these events. Detection of hot spots in the Brazilian Cerrado and Tropical Forest using AVHRR (Advanced Very High Resolution Radiometer), aboard the NOAA polar orbiting satellites series, was developed by Pereira [26] and Setzer and Pereira [27]. Prins and Menzel [28] presented the monitoring of biomass burning in the Brazilian Cerrado and deforested areas using VAS (Visible Infrared Spin Scan Radiometer Atmospheric Sounder) on the GOES (Geostationary Operational Environmental Satellite). The technique is based on the difference of the radiative temperatures associated with the two infrared channels [29]. Although the low spatial resolution of the GOES VAS instrument was a limiting factor for monitoring biomass burning, the high temporal resolution was a great advantage, allowing detection of the diurnal variability of fire number and extent. The launch of the GOES-8 Imager in 1994, and the implementation of the ABBA (Automated Biomass Burning Algorithm, version 1.1) for the 1995 biomass burning season represented a significant improvement in South American active fire monitoring [5]. The resolution of the GOES Imager at nadir (sub-satellite point) is 1 km in the visible and 4 km in the 3.9 and 10.7 micron infrared bands. The instantaneous ground fields of view (IGFOV) are oversampled in the east/west direction by a factor of 1.75 in the visible and IR bands providing a sampled resolution of 0.57 km in the visible band and 2.3 km in the infrared bands at nadir. This oversampling in the east/west can be used to enhance the apparent spatial resolution and allows for increased opportunity to capture an entire fire within one field of view. The ABBA algorithm was developed at UW-Madison CIMSS (Cooperative Institute for Meteorological Satellite Studies) to detect and estimate the size and temperature of biomass fires in South America automatically. Validation tests using prescribed fires in Rondônia State (Northwestern Brazil) reinforced the capability of the ABBA algorithm to identify and estimate instantaneous fire temperature and size for fires on the order of a few acres. Nevertheless, inaccurate corrections for cloud contamination and atmospheric attenuation can produce overestimates of the fire size. A study of the diurnal variability of the

detected number of fire pixels for the 1995 burning season showed that the peak of burning occurs around 17:45 UTC and ranged between 1500 and 3500 fire pixels. The number of fires detected at 17:45 UTC is from 3 to 4 times larger than the number of fires at 14:45 and 20:45 UTC and about 20 times greater than the number of fires detected at 11:45 UTC [30]. A new version of the GOES-8 ABBA was developed for fire detection and monitoring throughout the Western Hemisphere. The Wildfire ABBA (WF_ABBA) enables fire monitoring in most ecosystems and was streamlined to allow for rapid processing of half-hourly GOES Imager data for hazards applications and model data assimilation activities. Version 6.0 of the WF_ABBA was implemented during the 2002 fire season in South America.

Biomass burning emits hot gases and particles which are transported upward due to positive buoyancy. The interaction between the smoke and the environment produces eddies that entrain colder environmental air into the smoke plume, which dilutes the plume and reduces buoyancy. The daily turbulent transport in the planetary boundary layer (PBL) produces a well-mixed layer; while horizontal advection transports the plume downwind in the PBL. Dry and wet convective processes and topographic forcing transport tracers into the middle and upper troposphere. In the troposphere, the pollutants are advected away from the source region. Removal processes are more efficient in the PBL; when the pollutants are transported to the troposphere their residence time increases. Several authors [16, 17, 31–39] have been working on the transport of biomass burning emissions in the South American and African continents, mainly focusing on the transport due to wet and deep convective circulations. They have shown the importance of this mechanism on the vertical distribution of the biomass burning pollutants from the PBL to the high troposphere with possible implications for regional and global climate change.

3. The Atmospheric and the Coupled On-Line Eulerian Tracers Transport Models

The on-line 3-D model transport follows the Eulerian approach coupled to the RAMS 4.3 parallel version [21]. RAMS is a numerical model designed to simulate atmospheric circulations at many scales. RAMS solves the fully compressible non-hydrostatic equations described by Tripoli and Cotton [40], and is equipped with a multiple grid nesting scheme which allows the model equations to be solved simultaneously on any number of interacting computational meshes of different spatial resolution. It has a sophisticated set of packages to simulate processes such as: radiative transfer, surface-air water, heat and momentum exchanges, turbulent planetary boundary layer transport and cloud microphysics. The initial conditions can be defined from various observational data sets that can be combined and processed with a mesoscale isentropic data analysis package [41]. As for the boundary conditions, there is a 4DDA (four-dimensional data assimilation) scheme allowing the atmospheric fields to be nudged towards the large-scale data.

During the dry season, South America and Africa have a large number of vegetation fires throughout much of the continent. The effects of these fires on the lower-middle and upper troposphere are expressed very discretely by cloud transports. The computational limitation constrains the model runs to low spatial resolution (on the order of a few tens of kilometers). At this resolution, a cumulus scheme parameterization needs to be introduced because the model is not capable of resolving convection explicitly. New deep and shallow convective parameterization schemes based on a mass flux approach [42, 43] have been implemented in RAMS 4.3. The Grell scheme includes moist convective-scale downdrafts and uses as closure the quasi-equilibrium hypothesis for the determination of the updraft mass flux on the cloud base. This cumulus scheme is suitable for mesoscale runs (horizontal grid spacing about 20 km) and so is adequate for regional transport studies.

The tracer mixing ratio, $s(= \rho/\rho_{\text{air}})$, is calculated using the mass conservation equation

$$\frac{\partial s}{\partial t} = \left(\frac{\partial s}{\partial t}\right)_{\text{adv}} + \left(\frac{\partial s}{\partial t}\right)_{\substack{\text{PBL}\\ \text{turb}}} + \left(\frac{\partial s}{\partial t}\right)_{\substack{\text{shallow}\\ \text{conv}}} + \left(\frac{\partial s}{\partial t}\right)_{\substack{\text{deep}\\ \text{conv}}} + W_{\text{PM2.5}} + R + Q, \tag{2}$$

where the symbols are defined as follows:

- $\frac{\partial s}{\partial t}$, the local tendency,
- *adv*, the grid-scale advection,
- *PBL turb*, the sub-grid turbulent transport in the PBL,
- *deep conv*, the sub-grid transport associated with the moist deep convection,
- *shallow conv*, the sub-grid transport associated with the moist shallow convection,
- $W_{\text{PM2.5}}$, the convective wet removal for PM2.5 (particulate matter with $d_{\text{p}} < 2.5\mu\text{m}$),
- R, the sink term associated with generic dry removal and/or chemical transformation,
- Q, the source emission associated with the biomass burning process.

The tracer mixing ratio is updated in time using the total tendency given by Equation (2) and a constant inflow is applied as a tracer boundary condition. The next sections will discuss other terms on the right hand side of Equation (2) in more detail.

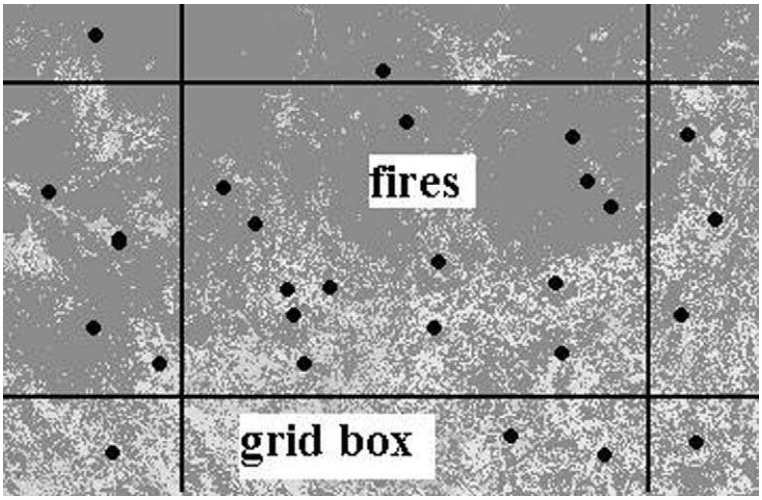

Figure 1. Biomass burning source emission parameterization. Fires are sub-grid processes burning different types of vegetation. The total amount of emitted mass is obtained and diluted in the air contained in each model grid box.

3.1. THE PARAMETERIZATION OF THE SOURCE EMISSION Q

The source emission parameterization is based on the half-hourly GOES-8 WF_ ABBA fire product and field observations. Figure 1 illustrates the technique. Inside of each model grid box there may be several observed sub-grid fires each burning a different type of vegetation. For each fire pixel detected by the GOES-8 WF_ABBA, the mass of the emitted tracer is calculated using Equation (1) where the type of vegetation burning is determined by merging the fire map with the 1 km IGBP 2.0 vegetation map [44], thus allowing an appropriate selection of the vegetation-dependent factors in Equation (1). We estimate the burned area by the instantaneous fire size given by the GOES-8 WF_ABBA for each non-saturated and non-cloudy fire pixel, where it is possible to retrieve sub-pixel fire characteristics. For GOES-8 WF_ABBA detected fires that have no information about the instantaneous fire size, the mean instantaneous fire size of 0.14 km^2 (calculated from the GOES-8 ABBA database of the previous years) is used. The emission in the model follows the diurnal burning cycle described in Section 2. The emission diurnal cycle is defined by a Gaussian function *r(t)* centered at 17:45 UTC, normalized to 1, and 8 h wide. In this way, the source emission term is given by

$$Q^{[\eta]} = \frac{r(t)}{\rho_0 \Delta V} \sum_{\substack{\text{fires\_}\in \\ \text{Grid\_Box}}} M^{[\eta]}, \tag{3}$$

where ρ_0 is the basic state air density, ΔV is the volume of the first physical grid cell (corresponding to the vertical level $k = 2$) and the mass is calculated over all fires inside the grid cell. The sources are spatially and temporally distributed

and daily assimilated by the model according to the biomass burning hotspots identified in the GOES 3.9 micron band by the WF_ABBA processing system. Presently, the source emissions for CO and PM2.5 have been parameterized, but several significant species could be added, e.g., CO_2, NO, HCN.

3.2. THE SINK TERM *r*

The generic process of removal/transformation of tracers (dry deposition and sedimentation for PM2.5 and chemical transformation for CO) is summarized through the term R given by

$$R = -\frac{s}{\lambda}, \tag{4}$$

where the lifetime λ is approximated as 30 days for CO [45] and 6 days for PM2.5 [2]. Since the lifetime of CO is long, from 50 to occasionally a minimum of 15 days [46], CO acts essentially as a passive tracer in the simulation. The CO in the simulations tends to flow out of the model, especially above the boundary layer, and boundary conditions control the concentration more than the linearized chemical removal. Similarly, within the boundary layer, it is true that the transport time from the major sources to major vertical transport regions is shorter than 15 days, and so the exact lifetime assigned is of secondary importance. The PM2.5 tracer quantity represents a monomodal submicron aerosol not significantly affected by coalescence or condensation of further material. This seems to be an adequate description for smoke starting a few hours after emission through the point of significant interaction with cloud and a high probability of removal. Within the boundary layer, the 6-day lifetime for PM2.5 corresponds to a deposition velocity of $\sim$0.35 km/day within the approximately 2 km mixed layer. This value is perhaps three times the commonly used deposition velocity for small particles, and approximately correct for larger particles which have less mass efficiency in affecting light. Above the mixed layer, the suggested lifetime is too short, but here aerosol is dispersed more rapidly by winds, as with CO. The general effect should be that our removal is too rapid. More realistic dry deposition and sedimentation schemes will be implemented for operational monitoring during the next dry season. The major uncertainties in the mass loading and optical effects that we are addressing concern emission strength and wet removal efficiency, and these have the greatest impact on our model performance.

3.3. THE PARAMETERIZED DEEP CONVECTIVE TRANSPORT AND ASSOCIATED WET REMOVAL

The deep and moist convection effects on the tracers' distribution are based on the Grell mass flux cumulus scheme. This sub-grid transport tendency on the tracer mixing ratio is given by

$$\left(\frac{\partial s}{\partial t}\right)_{\substack{\text{deep}\\ \text{conv}}} = \frac{m_b}{\rho_0}\left[\delta_u \eta_u \left(s_u - \tilde{s}\right) + \varepsilon \delta_d \eta_d \left(s_d - \tilde{s}\right) + \tilde{\eta}\frac{\partial \tilde{s}}{\partial z}\right], \tag{5}$$

where m_b is the updraft mass flux at cloud base, δ is the mass detrainment rate and η is the normalized mass flux, with the subscripts u and d standing for updraft and downdrafts, respectively. ε is the ratio between the downdraft and updraft mass fluxes, $\tilde{\eta}$ is the environment normalized mass flux, s_u, s_d and $\tilde{s}$ stand for tracers mixing ratio for the in-cloud updraft, downdraft and environment, respectively. The first term on the right side of Equation (5) corresponds to updraft mass detrainment, the second, to downdraft mass detrainment, and the last, to environmental subsidence (advection). For biomass burning tracers usually the PBL is more polluted than the troposphere, so the typical role of the updraft transport is to vent the polluted air from the PBL to the high troposphere where the smoke-laden air is detrained. Conversely, the downdraft brings more pristine air from the mid troposphere into the PBL.

The in-cloud tracer mixing ratio is determined from

$$\frac{ds_{u/d}}{dz} = -\mu_{u/d}\left(s_{u/d} - \tilde{s}\right), \tag{6}$$

where $\mu_{u/d}$ is the up/downdraft entrainment rate and the following boundary condition is used

$$s\left(z_{u/d}\right) = \tilde{s}\left(z_{u/d}\right), \tag{7}$$

z_u is the updraft cloud base height, and z_d is the height level where the downdraft starts. The coupled convective tracers transport model utilizes m_b, $\delta_{u/d}$, $\eta_{u/d}$, $\tilde{\eta}$, ε, $\mu_{u/d}$, z_u and z_d diagnosed from the cumulus scheme to determine the value of Equation 5.

Wet convective removal for PM2.5 is parameterized following Berge [47]. The in-cloud scavenging (washout) is given by

$$W_{\text{PM2.5}} = -\frac{\chi s_u p}{m_W \Delta z}, \tag{8}$$

where χ is the scavenging efficiency, that is, the probability for aerosols to get embedded in cloud droplets which rain out. p and m_W are the precipitation rate and the liquid water content, respectively; and Δz is the thickness of the model layer. The estimated value for χ is between 0.53 and 0.71 for smoke [48], and the simple mean of 0.62 is used in the model. The precipitation rate and the liquid

water content are both diagnosed by the Grell cumulus scheme and in-cloud tracer concentration is obtained through Equation (6) after the washout. The sub-cloud precipitation scavenging (rainout) is estimated from

$$W_{\mathrm{PM2.5}} = -AMEs_u, \tag{9}$$

where M is the concentration of precipitation water (kg [water]/m^3), E is the mean collection efficiency averaged over all raindrop sizes and A is an empirical coefficient [47].

3.4. THE PARAMETERIZED SHALLOW CONVECTIVE TRANSPORT

The shallow convective transport follows the same approach described in Equation (5), but disregards the transport by downdrafts and the wet removal process. It is coupled to the Grell shallow convection scheme. Here, shallow cumuli act only in venting the aerosol particles and gases from the PBL to the low troposphere.

3.5. THE GRID SCALE ADVECTION AND SUB-GRID TURBULENT TRANSPORT

The grid scale advection and the sub-grid diffusional transport are calculated using existing RAMS parameterizations. The horizontal diffusion is based on the Smagorinsky [49] formulation. The vertical diffusion is parameterized according to the Mellor and Yamada [50] scheme, which employs a prognostic of the turbulent kinetic energy. The advection is a forward–upstream scheme of second-order [51].

4. Real Time Transport Monitoring

The operational system follows the scheme depicted in Figure 2. The fires observed by the GOES-8 WF_ABBA on the previous day and the tracers concentration of the last run provide the source emission and the initial condition for the tracers. The CPTEC (Center for Weather Prediction and Climate Studies-Brazil) global analysis and forecast provide the initial and boundary conditions for the regional atmospheric model using the 4DDA technique. The model configuration has 2 grids. The coarse grid has a horizontal resolution of 200 km (106×41 grid points) covering the South American and African continents. The source emission for the African vegetation fires is prescribed following the Emission Database for Global Atmospheric Research-EDGAR [52] since the GOES-8 does not observe this continent. Its main purpose is to simulate approximately the intermittent smoke inflow from the African fires to South America and to coordinate with and compare to the long-range transport of smoke from fires in South America to the Atlantic Ocean. The nested grid has a 40 km horizontal resolution (157×162) and covers only South America. The vertical resolution for both grids is between 150 to 850 m, with the top of the model at 21 km (33 vertical levels). Each time integration is 48 h (24 h of which is forecast). The integration was initiated on 1 July 2002 and carried

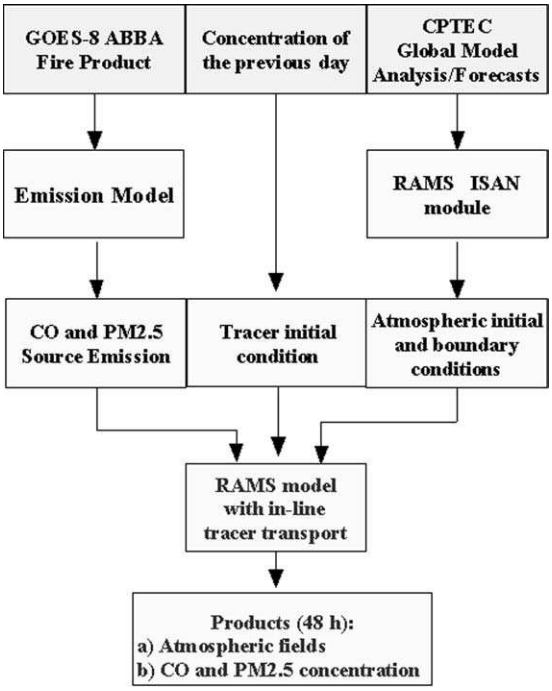

Figure 2. General flow of the real time system for monitoring the transport of biomass burning emissions in South America.

through successive 48-h integrations through 30 November 2002. This system has been running on a pc-Linux cluster with 13 processors (Intel-pentium III, 1 GHz) and takes about 5 h of computation time.

5. Discussion

Climatologically, from June to September, central Brazil is dominated by a high-pressure area with little precipitation and light winds in the lower troposphere [53] and with convection in the Amazon basin shifted to the northwest part of South America. These conditions are associated with the westward displacement of the South Atlantic Subtropical High (SASH) and the northward motion of the Intertropical Convergence Zone (ITCZ) during the austral winter. However, on a day-to-day basis several transient systems may change this picture, thereby altering the typical pattern of the smoke transport. The position of the SASH determines the entrance of the clean maritime air to the biomass burning area playing an important role in defining the shape of the regional smoke plume as it is the primary mechanism responsible for the dilution of the polluted air. Approaching cold frontal systems from the south are responsible for disturbances in atmospheric stability and in the wind fields. These changes define the main corridors of smoke export to oceanic areas. The typical model output representing the tracers (CO and

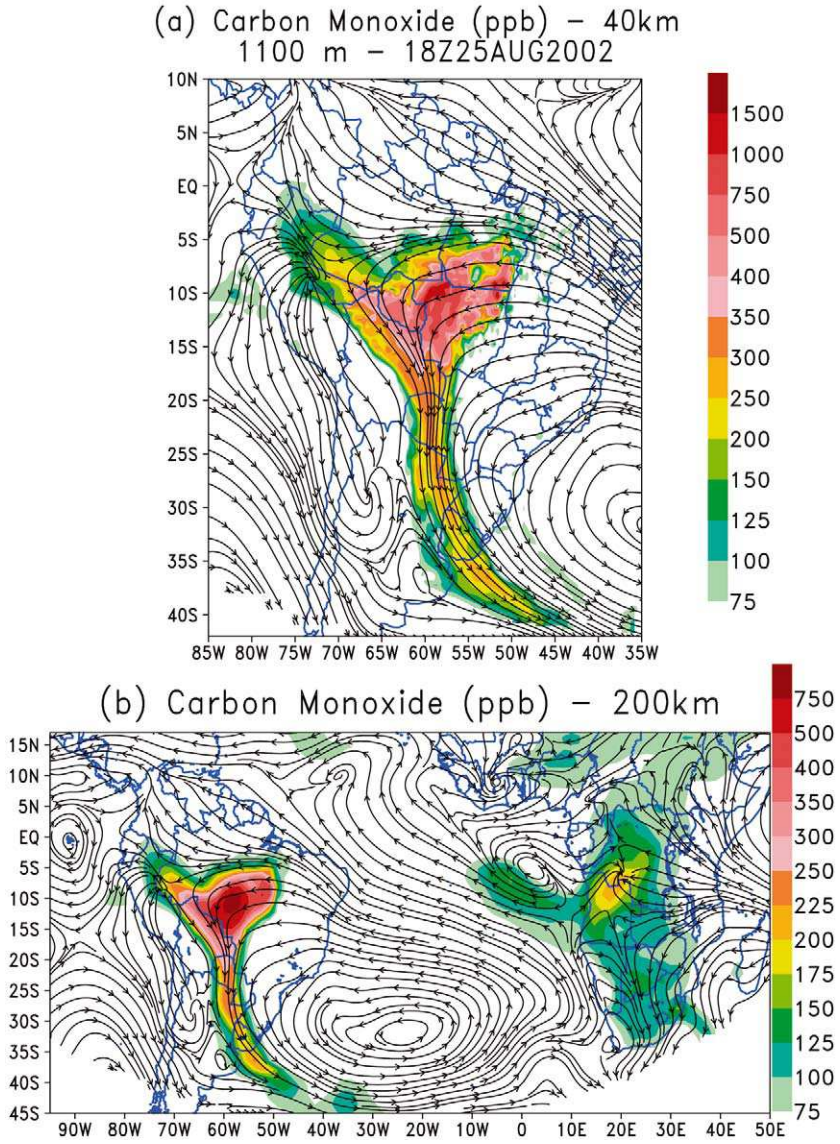

Figure 3. Example of the transport model output. (a) Shows the plume of CO (ppb) for the regional model grid (40 km horizontal resolution) at 1800Z on 25 August 2002 at 1100 m above surface. (b) Depicts the coarse model grid (200 km) covering South America and parts of Africa.

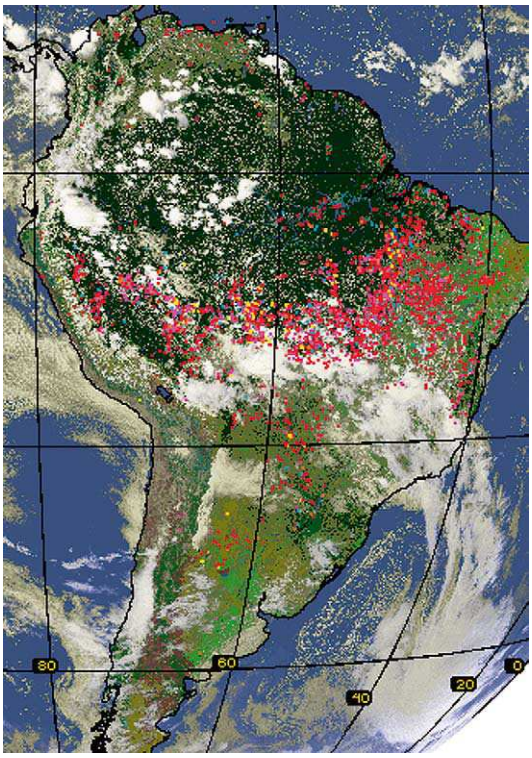

Figure 4. The GOES-8 WF_ABBA fire product at 1745 UTC on 7 September 2002 depicting the vegetation fires in South America. Also shown is the cloudiness associated with a cold front synoptic system impacting the polluted boundary layer.

P2.5) simulated distribution and wind fields express the connection between the atmospheric flows and the smoke transport.

Figure 3a shows the CO mixing ratio (ppb) at 1100 m above the surface level at 1800 UTC on 25 August on the regional grid with a spatial resolution of 40 km. The simulated regional smoke plume showed CO concentration values ranging from 100 to 1000 ppb, with maximum values over the places with the highest concentration of fire pixels. For PM2.5, the simulated values typically ranged from 10 to 500 μg m^{-3} at the surface level and from 10 to 200 mg m^{-2} for the integrated vertical column. A smoke corridor is evident and it was associated with anticyclonic circulation centered over the Atlantic Ocean. The long-range transport of smoke results in transboundary air pollution with smoke-laden air crossing into the South American countries of Paraguay, Argentina and Uruguay. Figure 3b shows the CO mixing ratio on a large-scale grid at a spatial resolution of 200 km. A small smoke plume located near latitude 45 S and longitude 35 W has traveled about 7000 km. Also seen is the transport of CO from African fires using the approximate sources of the time-invariant EDGAR inventory. While there was MOPITT data available (see http://www.eos.ucar.edu/mopitt/index.html) for this period, the simulated CO

was primarily in the boundary layer or hidden by cloud and largely invisible to the MOPITT sensor. MOPITT depends upon thermal emission of radiation from CO molecules, and is most sensitive in the mid troposphere. Estimates for lower tropospheric levels (below 2–3 km tend to represent a standard initial profile used for the retreival. The MOPITT estimate at 1.5 km suggests around 250 ppb for the portion of South America seen. In Africa, where climatological fire emissions had to be used, the comparison was of course not quite as good. More intensive comparisons between model and MOPITT results are in development.

5.1. A COLD FRONT CASE STUDY

This section describes the typical role of a mid-latitude cold front on smoke transport and distribution. Figure 4 presents the GOES-8 WF_ABBA fire product depicting over one thousand South American vegetation fires at 1745 UTC on 7 September 2002. Note also the cloudiness associated with a cold frontal system which is affecting a boundary layer polluted by fire emissions. The parameterized CO source emission for this day is shown in Figure 5. Some forest biomes in Brazil emitted over 2 ton km^{-2} of carbon monoxide. Figure 6a presents the wind field and the temperature (degrees Celsius, contour lines) at 875 m above the surface at 00 UTC on 7 September 2002 and shows a mass convergence line and an enhanced temperature gradient to the south of the convergence line. Shaded contours represent the vertically integrated PM2.5 mass concentration (mg m^{-2}). Anti-cyclonic flow behind the cold front was outlined after 30 hours of simulation (Figure 6b). The model simulation shows good agreement in the location of convection and timing of the precipitation estimated by the Tropical Rainfall Measuring Mission (TRMM, http://trmm.gsfc.nasa.gov). An example for 7 September of the 24 hour accumulated rainfall (mm) 25-km resolution TRMM product and as simulated by the model, including the explicitly resolved and the convective parameterized, are shown in Figures 7a and b, respectively. The model spatial distribution suggested more widespread rainfall in the northern ocean regions (around 10 N) than determined by TRMM. The model also simulated less rainfall in some areas of the continent (around 20 S and 5 S). Some of this mismatch might be due to the difference in the horizontal resolution of the two data sets.

The most evident effect of a cold front approaching Central Brazil is the northward transport of the regional smoke plume. Following the cold front approach, the polluted air in central South America is replaced by a clean and cold air mass. The smoke is then pushed into the Amazon basin, changing the pristine air composition. This could have both climatic and chemical implications. During these events, it was also observed that the transport of smoke to the Pacific Ocean was enhanced. Less obvious is the effect of the associated convective systems on the particulate and gaseous distribution, as it involves an enhancement of the vertical transport and precipitation and subsequent smoke scavenging, including NO_x deposition (via soluble nitric acid). Figure 8a is a vertical cross section at latitude 13 S showing

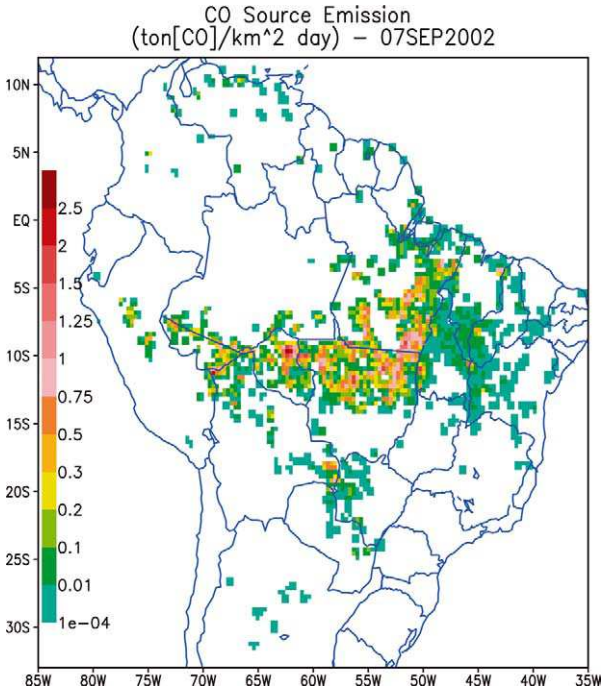

Figure 5. The parameterized CO source emission for 7 September 2002. Some areas in Brazil with forest biomes emitted over 2 ton km^{-2} of carbon monoxide.

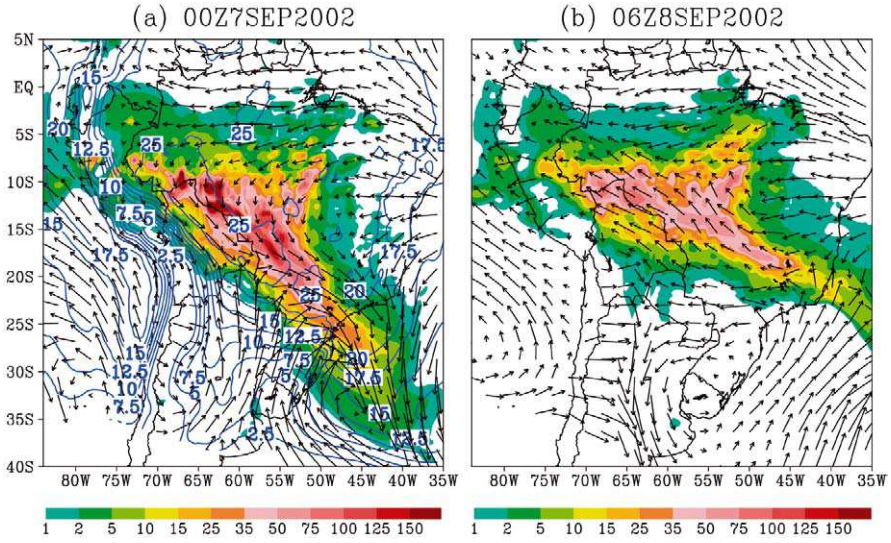

Figure 6. (a) Wind field and temperature (degrees Celsius, blue contour lines) at 875 m above the surface at 00Z on 7 September. Shaded contours represent the vertically integrated PM2.5 mass concentration (mg m^{-2}). (b) Wind field and PM2.5 mass concentration at 06Z on 8 September.

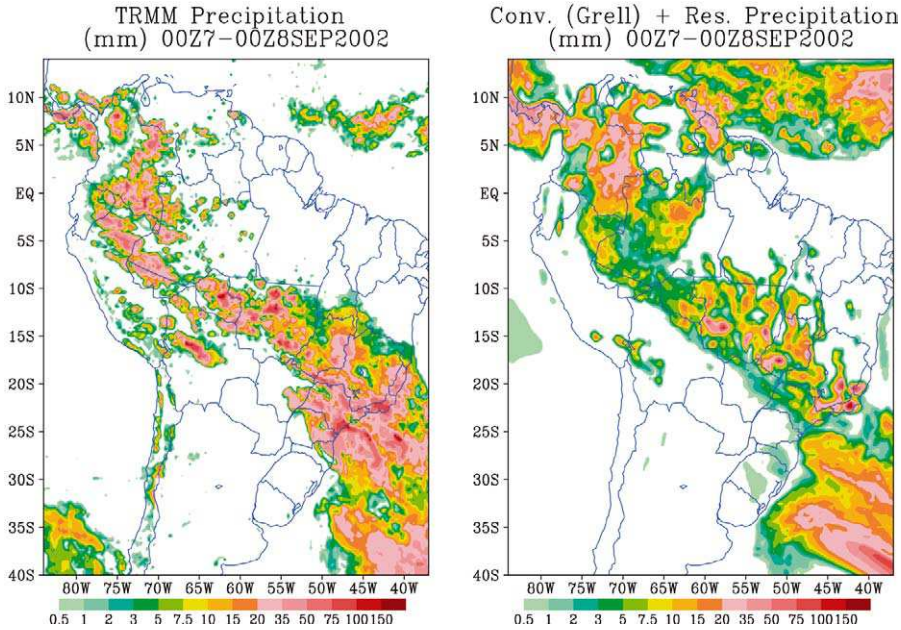

Figure 7. (a) Accumulated rainfall (mm) on 7 September as observed by the Tropical Rainfall Measuring Mission (TRMM), (b) RAMS model simulated (convective (Grell) plus resolved) rainfall for the same period.

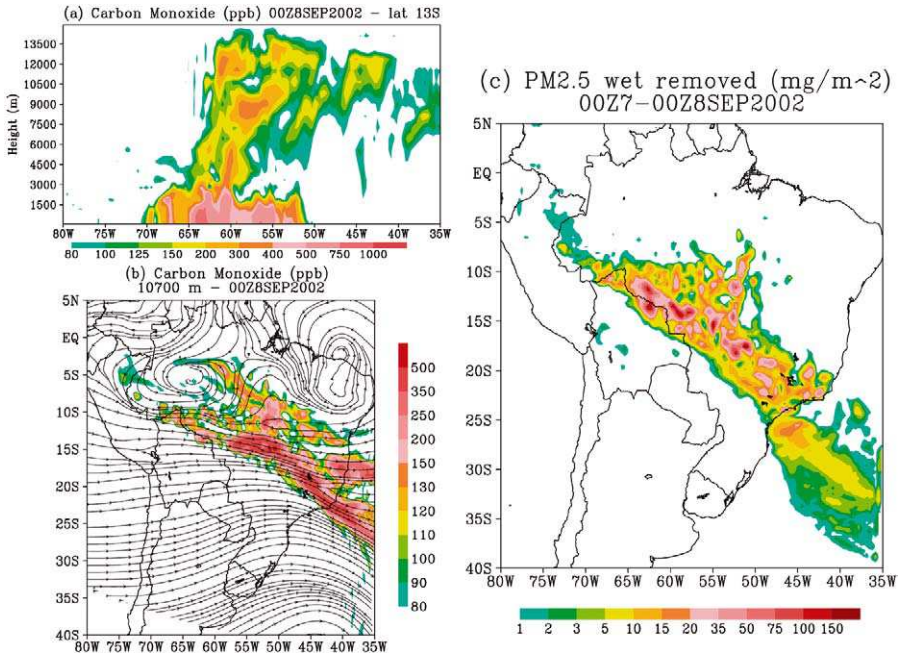

Figure 8. (a) Vertical cross section at latitude 13 S of CO (ppb) concentration in the PBL and the vertical transport of CO to the high troposphere at 00Z on 8 September. (b) Plume of CO at the 10700 m level (∼250 mbar) being advected by the zonal flow. (c) Accumulated PM2.5 wet removal (mg m^{-2}) between 00Z on 7 September and 00Z on 8 September.

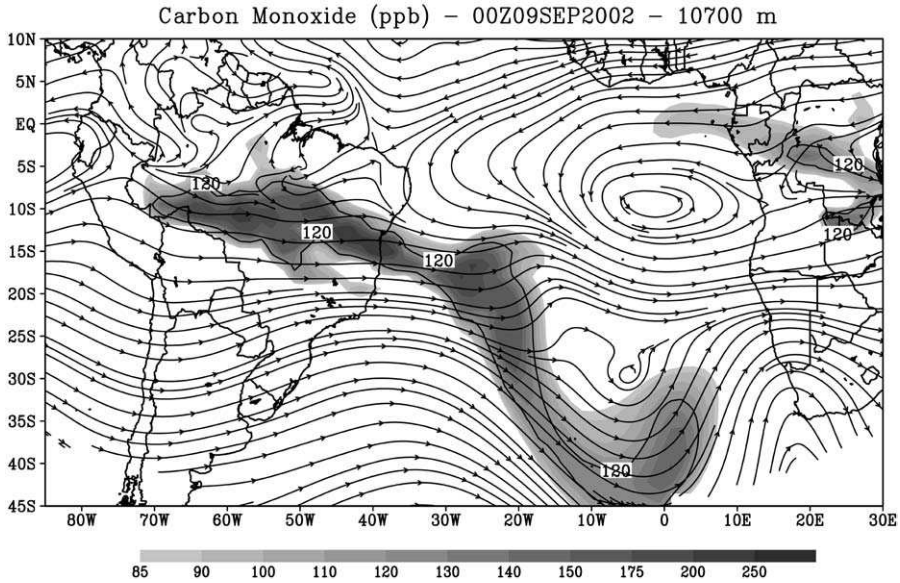

Figure 9. The long-distance transport of the CO plume at 10700 m above surface at 00Z on 9 September on the coarse resolution grid.

the high CO concentration in the PBL and the vertical transport of CO to the high troposphere by convective systems associated with the cold front. Values over 150 ppb are detrained between a height of 9 and 13.5 km. Figure 8b shows the plume of CO at the 10700 m (∼250 mbar) level being advected by the zonal flow. These simulations agree very well in both the general pattern and in magnitude with the MOPITT estimated CO for the day. For PM2.5, since it is mainly scavenged by rainfall, the main effect is its deposition over the continent and Atlantic Ocean (Figure 8c); this might have implications biogeochemical cycling of nutrients like fixed nitrogen. The long-distance transport of gaseous material poorly removed by clouds (and by extension, any similar non-scavenged aerosol) can be seen in Figure 9. After a cold front event, the high tropospheric plume crosses the Atlantic Ocean reaching the African continent, typically, one day later. The MOPITT data for the period suggest slightly lower values, but sampling conditions result in large portions of the plume not being observed.

5.2. MONTHLY TOTAL AND MEANS: GENERAL EXPORT PATTERNS

A South American map, including the model topographic field is provided in Figure 10 as a reference for further discussion. The Andes Mountains, Roraima Mountains and the Amazon basin are depicted, as well as, some Brazilian states (MT for Mato Grosso, RO for Rondônia and PA for Pará), some cities (TA for Tabatinga, SP for Sao Paulo and PtA for Porto Alegre) and, finally, the Jaru forest reserve (JA at Rondônia State).

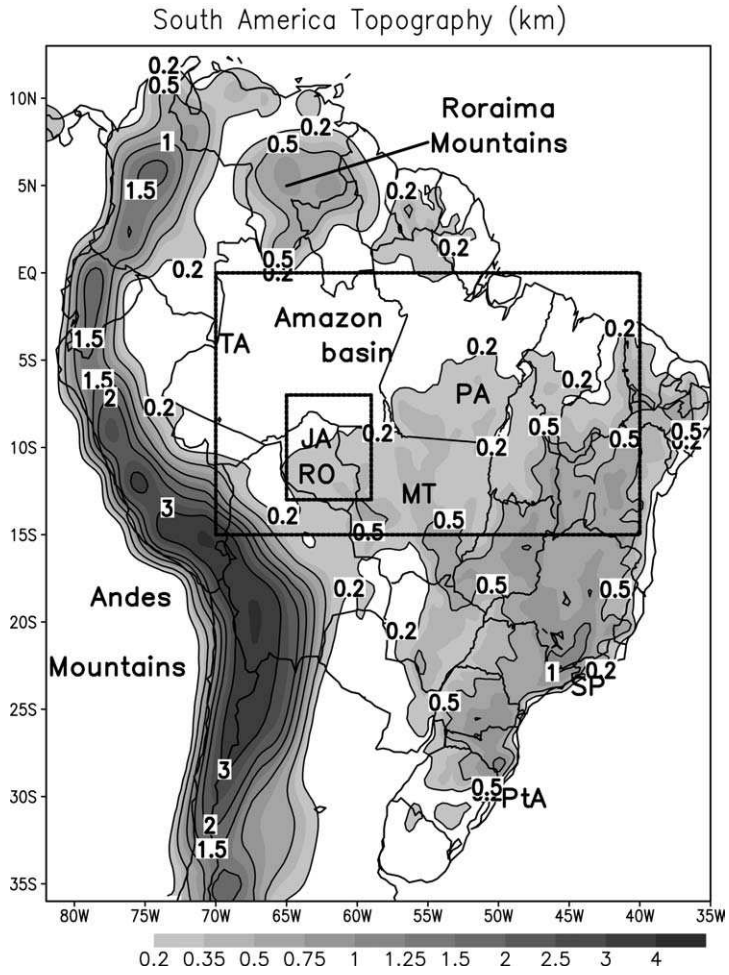

Figure 10. South America topography data for the 40 km horizontal resolution model grid. The primary regional burning area and Rondônia State are also depicted on the map.

Figure 11 shows the accumulated carbon monoxide emitted mass (in units of ton $km^{-2}month^{-1}$) for the months of August (a), September (b) and October (c) 2002. It depicts the places in South America where vegetation fires were observed by the GOES-8 WF_ABBA and the amount of CO introduced in the atmosphere as prescribed by the biomass burning emission model. In spite of the large number of fires detected in savannas and pastures, as compared to the number of forest fires, the greatest amount of the tracers came from forest fires, since the emissions are dependent on the fuel biomass density. Most of these locations are contoured as 5 ton km^{-2} $month^{-1}$. Some regions like Araguaia Valley (around latitude 9S and longitude 51W) emitted over 70 ton $km^{-2}month^{-1}$ of CO in August, indicating intense deforestation processes, according to the vegetation map. The Brazilian state Mato Grosso (MT) was the primary emission source over all months, followed by the

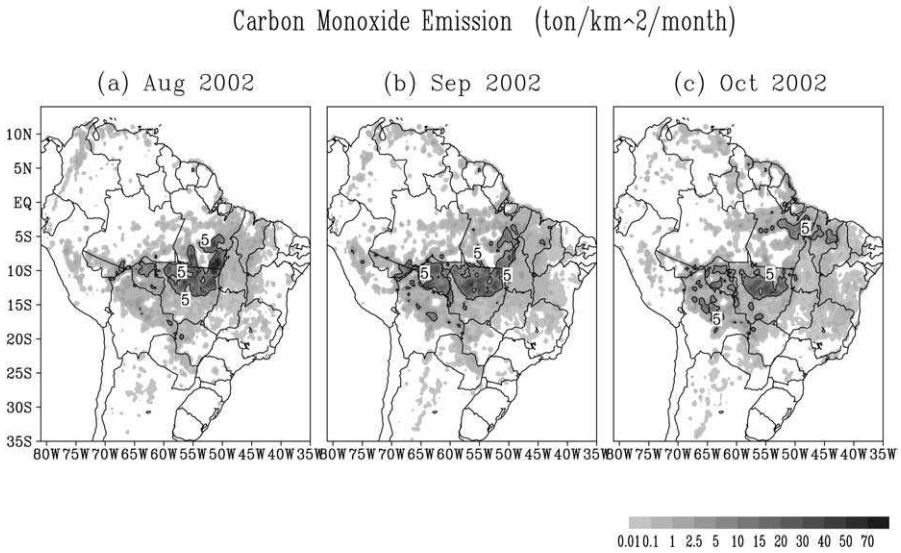

Figure 11. Accumulated carbon monoxide emitted mass (ton $km^{-2}month^{-1}$) for the months of August (a), September (b) and October (c) 2002 as prescribed by the emission model.

states of Para (PA) and Rondônia (RO). After Brazil, Bolívia was the country with the second highest biomass burning tracer emissions in South America, primarily in the month of October. In addition, in October, an important emission was noted in North-Northeast Brazil, resulting from deforestation processes in the transition zone between forest and caatinga (the predominant Brazil Northeast biome).

The monthly means of wind field (at 1100 m above the surface) and PM2.5 (vertically integrated, mg m^{-2}) on the large-scale grid (200 km horizontal resolution) are shown in Figure 12. Most of the mean transport pattern may be explained in terms of the trade winds, the South Atlantic subtropical high pressure system, and the barrier effect of the Andes Mountains. Most of the smoke in the lower troposphere was exported to the Atlantic Ocean through the southeastern part of South America. In August and September, a small amount of smoke was exported around latitude 8 S to the Pacific Ocean. In September weaker trade winds produced a more spread out plume compared with the August and October patterns. In October more intense meridional flow resulted in significant transport of smoke to the south of South America. During October, additional inflow of smoke into South America from African fires was observed. The pattern of transport to the west near the equator is much stronger in Africa than in South America, emphasizing the importance of the Andes Mountains. On a day to day basis, the transport pattern changed due to the occurrence of transient systems such as mid-latitude cold fronts or low level jets on the East side of the Andes Mountains.

The monthly meridional and zonal PM2.5 mass fluxes (in units of μg m^{-2} s^{-1}) are discussed in the following paragraphs.

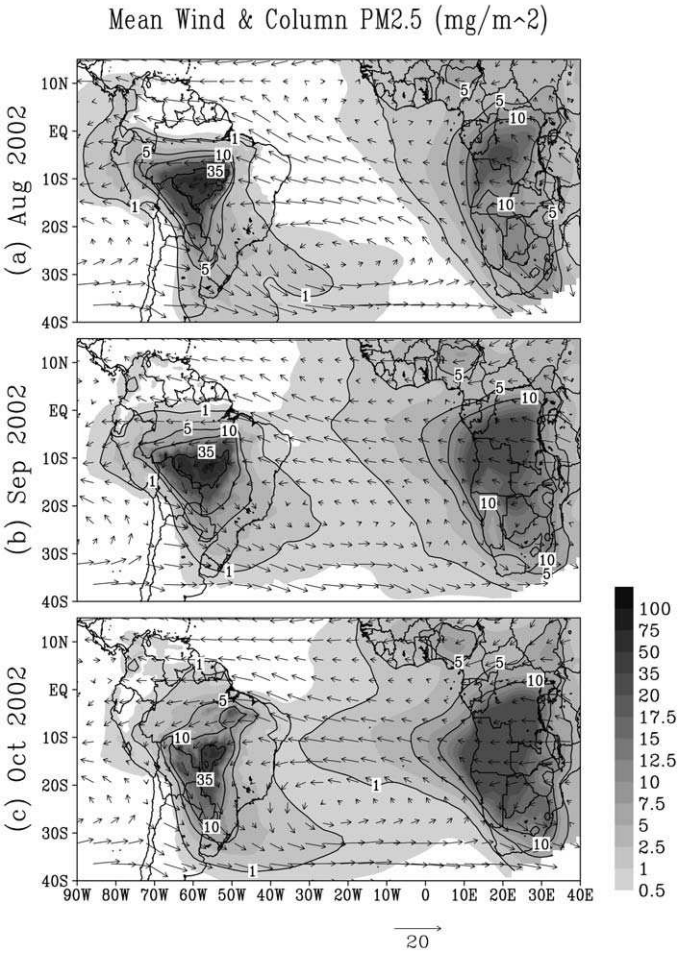

Figure 12. Monthly means of wind field (at 1100 m above the surface) and PM2.5 (vertically integrated, mg m^{-2}) on the large-scale grid (200 km horizontal resolution) for the months of August (a), September (b) and October (c) 2002.

Figures 13a, c and e show the monthly zonal flux at longitude 40 W and between latitudes 42 S and 10 N. The vertical axis is the height (m) above the local surface and the sign convention is positive for eastward fluxes. With the exception of September, the maximum zonal fluxes are around 2400 m in elevation. September had the maximum around 4000 m (not shown). These fluxes are mainly related to the occurrence of cold front synoptic systems, when the smoke exits South America ahead of these systems and towards the East. One can also observe that the association of the inflow zonal fluxes to the recirculation and transport from African fires emissions is primarily near the surface. We note again that in October the inflow from Africa is much more pronounced. The meridional fluxes at 35 S are shown in Figures 13b, d and f. In August there was a very strong channeled

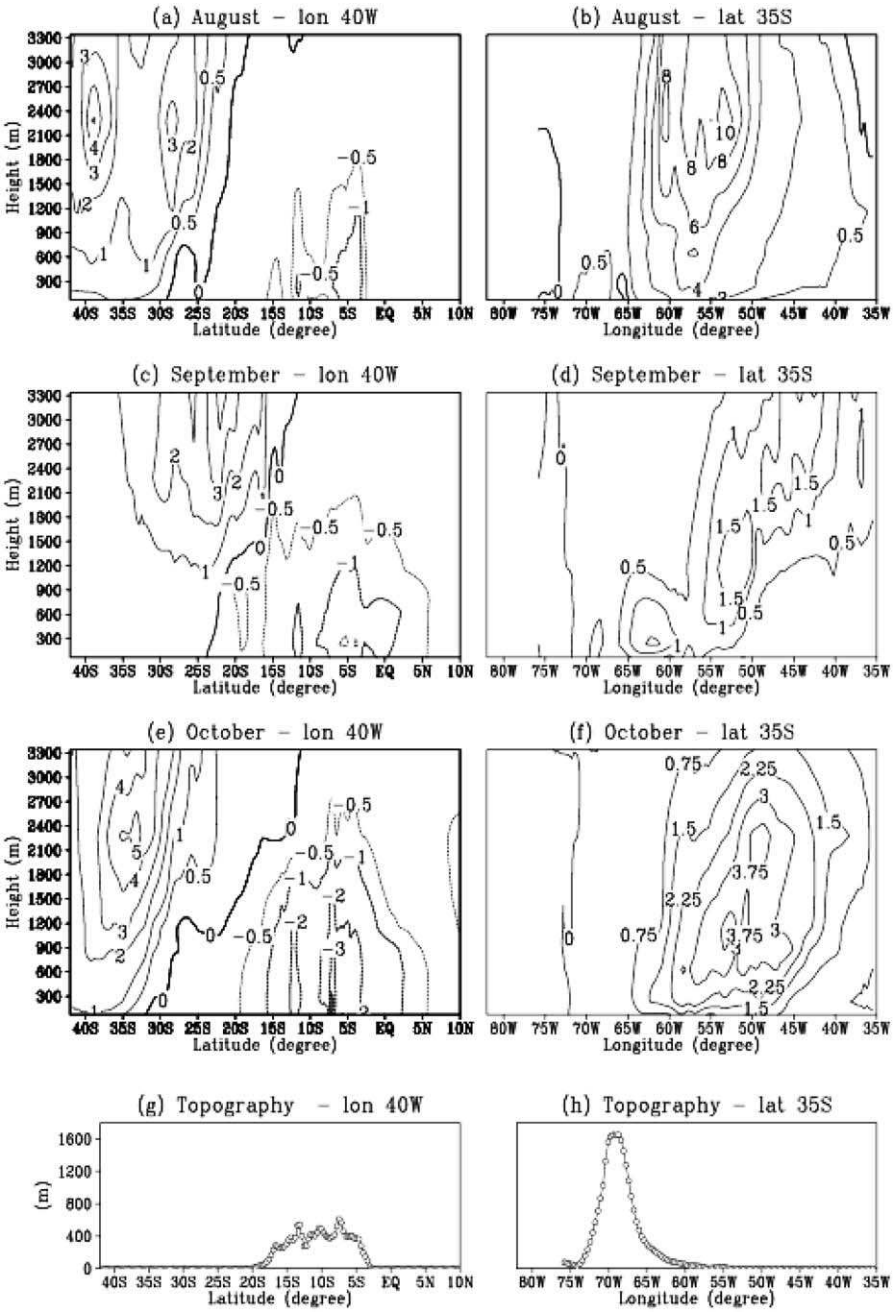

Figure 13. Monthly meridional and zonal PM2.5 mass fluxes (μg m^{-2} s^{-1}): (a), (c) and (e) show the monthly zonal flux at longitude 40 W and between latitudes 42 S and 10 N against the height (m) above surface; (b), (d) and (f) show the meridional fluxes at latitude 35 S. The terrain height profile is shown in (g) and (h). The signal convention is positive values for the outward fluxes.

mean flux up to 10 μg m^{-2} s^{-1} around 55 W and at a height of 2400 m, largely related to the Andes low level jets as shown in Figure 3. The other months had lower meridional fluxes which were more spread out.

Figure 14 shows the same fluxes as described in the last paragraph, but at longitude 82 W and the Equator. The transport to the Pacific Ocean took place predominantly around latitude 8 S (Figures 14a, c and e) and during the month of August. The meridional outward fluxes crossing the Equator (Figures 14b, d and f) are due to the channeling of the trade winds Northwest of the Amazon Basin by the Andes Mountains to the West and the Roraima Mountains to the East (as shown in Figure 3).

A different view of model performance is given by observations made at the surface. Time series of vertically integrated (mg m^{-2}) PM2.5 and CO (ppb) below 3300 m, as simulated by the model, are shown in Figures 15 and 16 for the sites Tabatinga (a), Jaru Reserve (b), São Paulo (c) and Porto Alegre (d) (see Figure 10 for their locations). Tabatinga is in the northwest Amazon and is used to monitor the incursion of smoke into the pristine areas of the Amazon basin. The smoke intrusion is well defined by the spikes of the PM2.5 column (Figure 15a) and the vertical profiles of CO (Figure 16a). Jaru Reserve is located within a burning region and serves as a local air quality indicator. Very strong boundary layer pollution was observed during August and September, reaching 250 mg m^{-2} and 2000 ppb for the particulate and CO concentrations, respectively (Figure 15b and Figure 16b). In October, with the onset of the rain season, the smoke was sharply reduced, showing only short-duration smoke bursts, mainly related to the local emissions. The cities of São Paulo and Porto Alegre (Figures 15 and 16c, d) are included to illustrate the South American smoke outflows and the effects of the regional smoke plume on the air quality of these cities. The narrow spikes of smoke passing over these cities are evident and were primarily associated with the convergence flows due to approaching cold fronts. The smoke plumes typically passed over the cities almost uncoupled from the surface and may have had insignificant effects on the local air quality. A strong outflow passing over Porto Alegre during October is shown in Figure 12c.

The connection between the narrow spikes of smoke in the time series for the Northwest and Southeast sites, which describes the continental export of smoke, can be envisioned by studying a sequence of events from 25 August to 3 September. Starting on 25 August (Figure 3a), the corridor of smoke was pushed towards the Andes Mountains due to a westward motion of the anti-cyclonic circulation, bringing clean oceanic air to the East and most of Central Brazil. On 28 August, a mid-latitude cold frontal system approached from the Pacific Ocean, pushing the smoke corridor back to the Atlantic Ocean (not shown). At 0600 UTC on 29 August the smoke corridor crossed the lower troposphere over Porto Alegre, as is indicated by the narrow spike preceding September 1 in Figure 15d. As the cold frontal system moved northward, the smoke corridor at the flow convergence region was pushed to the northeast and, one day later, was crossing São Paulo, as

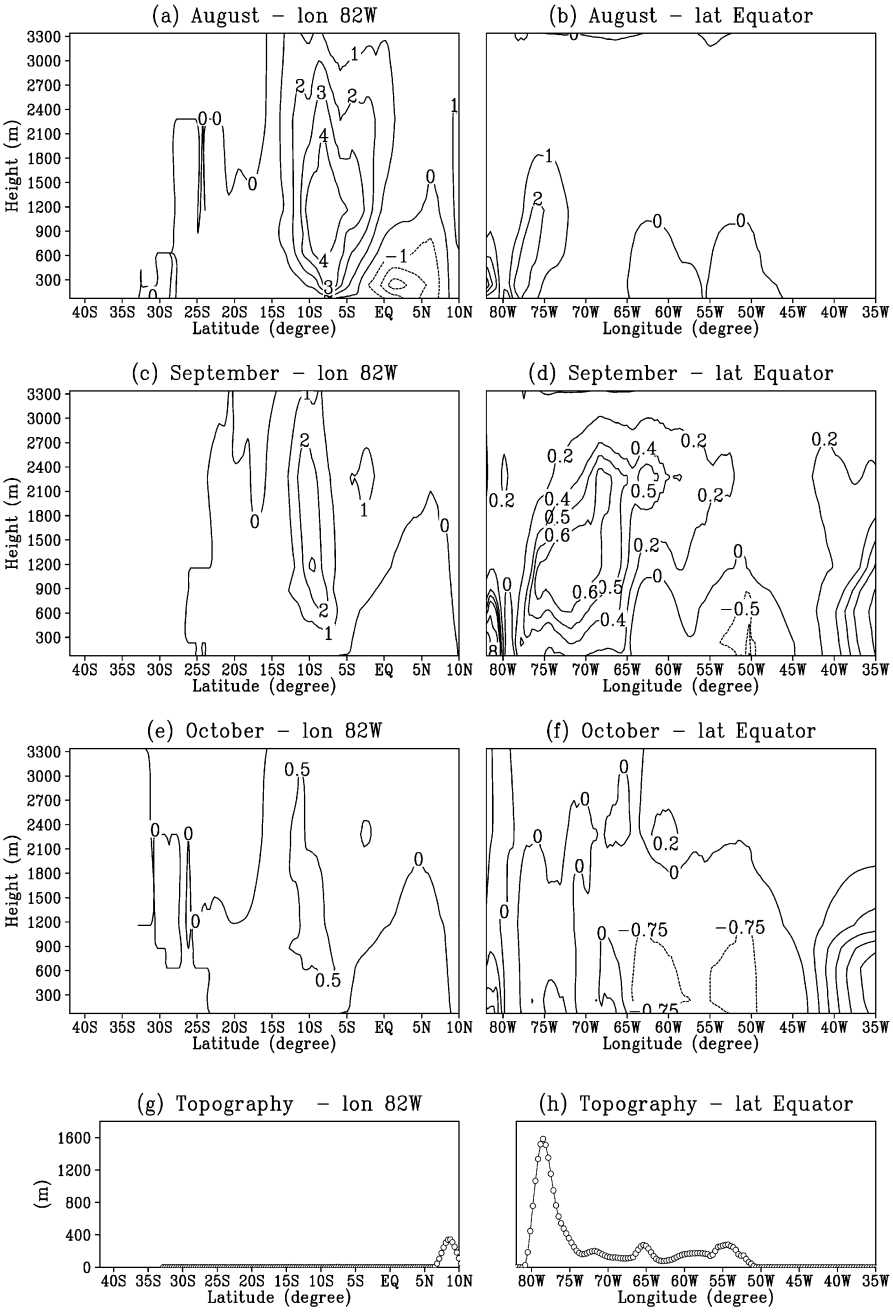

Figure 14. Monthly meridional and zonal PM2.5 mass fluxes (μg m^{-2} s^{-1}): (a), (c) and (e) show the monthly zonal flux on longitude 82 W and between latitudes 42 S and 10 N against the height (m) above the local surface; (b), (d) and (f) show the meridional fluxes at the Equator. The terrain height profile is shown at (g) and (h). The signal convention is positive values for the outward fluxes.

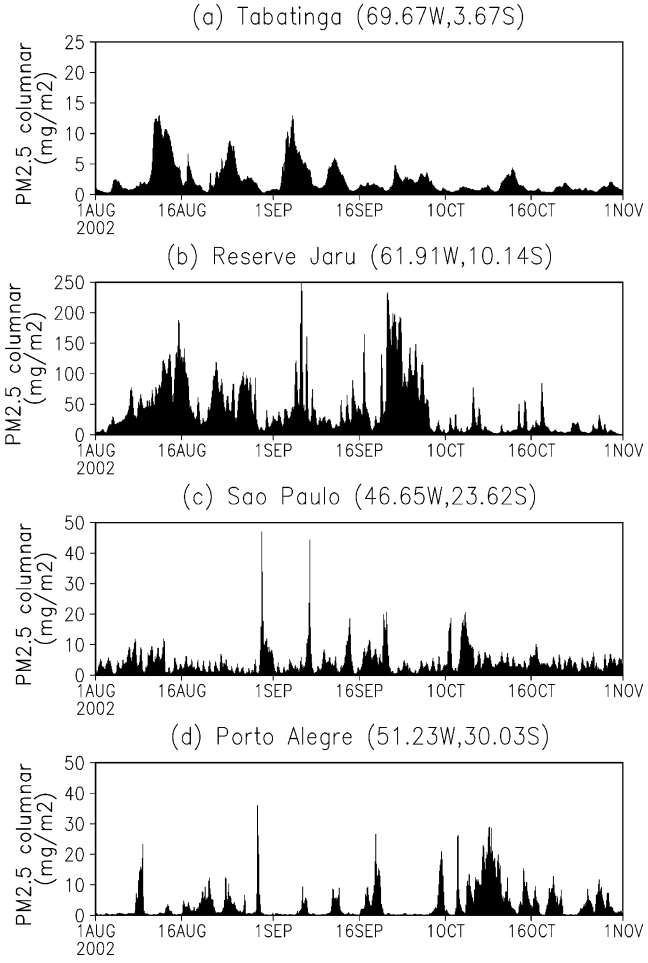

Figure 15. Time series of PM2.5 vertically integrated (mg m^{-2}) for the sites Tabatinga (a), Reserve Jaru (b), São Paulo (c) and Porto Alegre (d). Model results for the period 1 August – 31 October 2002.

indicated in Figure 15c. At the same time, the winds on the Jaru Reserve were from the northwest bringing pristine air from the Amazon basin, which explains the low smoke concentration around 1 September as depicted in Figure 15(b). As the cold front proceeded, it pushed smoke into the Amazon basin, which was followed by northwest transport by the trade winds. This explains the smoke plume at Tabatinga (Figures 15a and Figure 16a) around 3 September.

5.3. MEASUREMENTS AND MODEL COMPARISON

Aerosol measurements were made at the Ji-Parana pasture site, in the Rondônia state, approximately 90 km Southeast of the Jaru Reserve, during the Smoke Aer-

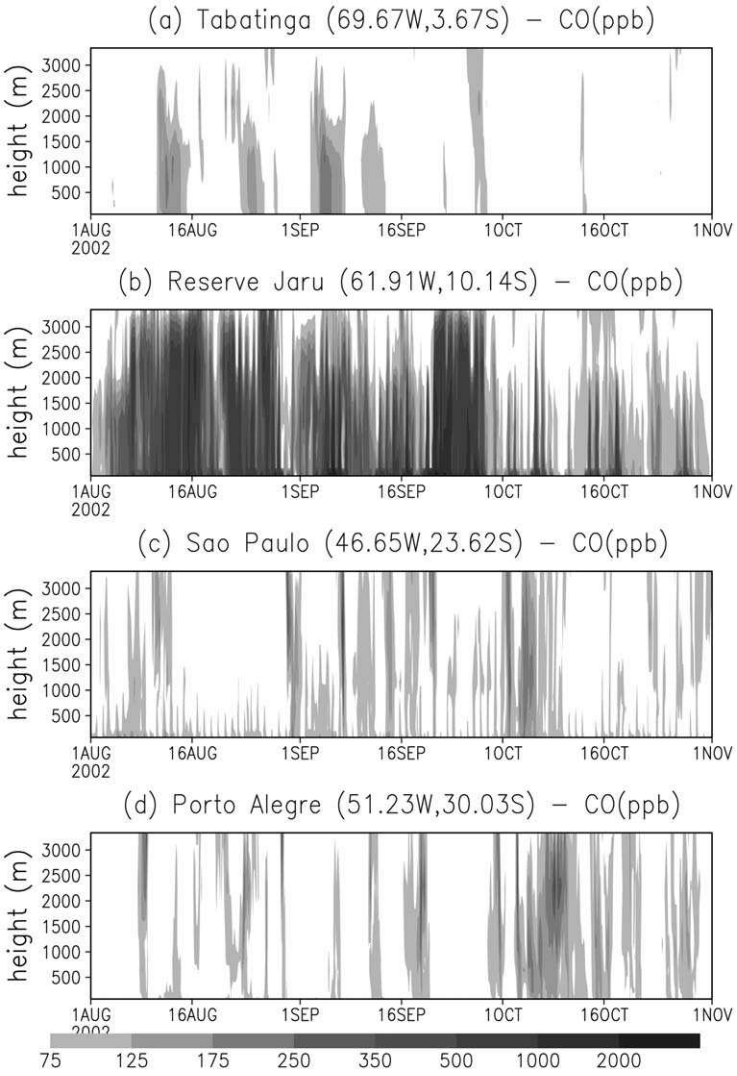

Figure 16. Carbon monoxide (CO, ppb) at 3300 m above the local surface for the sites Tabatinga (a), Reserve Jaru (b), São Paulo (c) and Porto Alegre (d). Model results for the time period 1 August – 31 October 2002.

osols, Clouds, Rainfall and Climate experiment (SMOCC, http://dionysos.mpch-mainz.mpg.de/smocc). The PM2.5 particle mass concentration was measured with a TEOM-instrument (Tapered Element Oscillation Mass Balance) at the surface with a 30-minute temporal resolution from 10 September to 4 November 2002.

During the SMOCC field campaign three very well characterized regimes of rainfall were observed. The period from 10 September to 8 October still shows the dry season characteristics with low precipitation rates and a high number of fires, not only in the Rondônia state but all over the Amazon basin and central

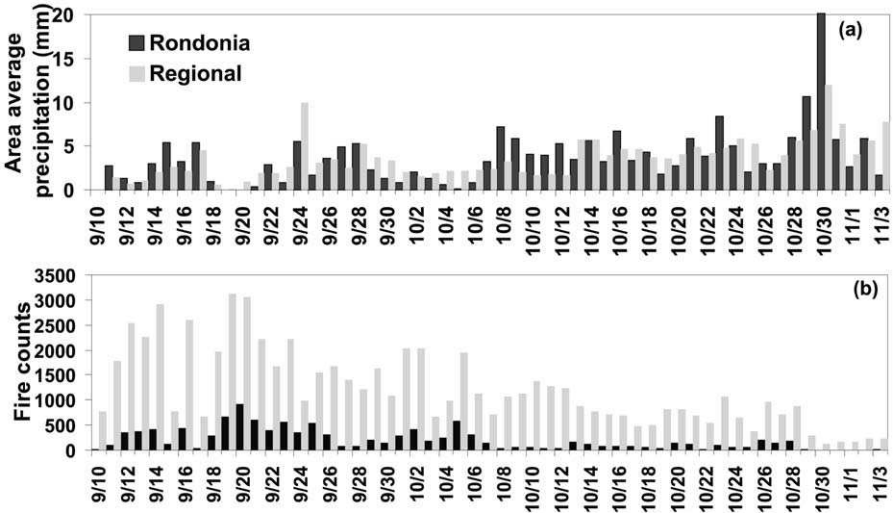

Figure 17. Time series of the (a) area average precipitation (mm) and (b) GOES-8 WF_ABBA fire counts over a 6° by 6° grid around the observation site at Rondônia and over a larger regional grid (21° by 10°) covering most of the frequent fire area. Both grids are depicted in Figure 10.

Brazil. From 8 to 30 October there was an increase in precipitation and a consequent reduction in biomass burning. In Rondônia state the fires were rare but fires were still observed in the regional area. By the end of October the onset of the wet season drastically reduced the number of fire counts everywhere in South America. This pattern is pictured in Figure 17, where time series of the daily fire counts from WF_ABBA and the area average of the estimated precipitation from the Global Precipitation Climatology Project (GPCP, http://precip.gsfc.nasa.gov) over the primary regional burning area and Rondônia state are shown. The primary regional burning area comprising a substantial part of the Amazon basin, central Brazil, and Rondônia state (RO) are depicted in the Figure 9.

This pattern is clearly reflected in the surface level aerosol particle measurements performed in Rondônia. During the most polluted period, high values of mass particle concentration were observed. The maximum values were as high as 210 μg m^{-3}, and the time series was characterized by strong variability. The diurnal evolution of the boundary layer contributes to this high variability. The variability mainly indicates the proximity of fires to the measurement site; the plumes are intense and still have not been significantly dispersed. During the transition and wet periods, with the reduction of burning around the measurement site, the mass concentrations were on average around 20 μg m^{-3} and 8 μg m^{-3}, respectively. An intercomparison of the PM2.5 mass concentration model results at 12Z with the daily average of the measurements values centered at 12Z reveals good agreement in terms of the general pattern of the temporal evolution, nevertheless the model values were systematically below the observation (Figure 18). A linear

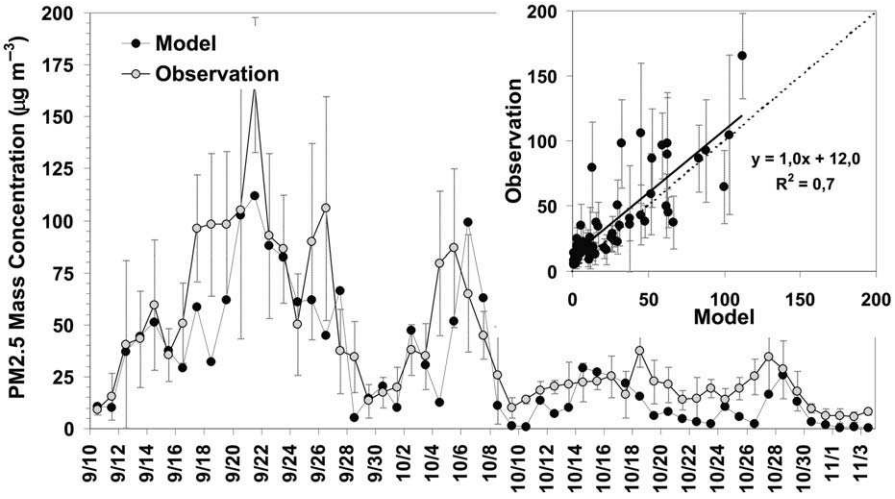

Figure 18. Time series of the PM2.5 mass concentration (μg m^{-3}) as simulated by the model (black) and measured with a TEOM-instrument (Tapered Element Oscillating Mass Balance) at the surface (gray) at the Ji-Paraná site in Rondônia. An inset scatter plot shows a linear regression of the PM2.5 mass concentration observed values versus modeled values. The measurements were daily averaged and centered at 12Z. The error bars are the standard deviations of the mean values. The model results are presented as instantaneous values at 12Z.

regression (inset to Figure 18) of the PM2.5 mass concentration observed values versus modeled values ($r^2 \approx 0.7$) confirms that the measurements tend to be higher than the model by a constant value of approximately 12 μg m^{-3}, which basically characterizes the background of mass particle concentration at Ji-Parana.

6. Conclusions

A tracer transport model fully coupled to a regional atmospheric model has been described. An emission model associated with remotely sensed vegetation fires was constructed, and a real time operational system was designed to monitor the biomass burning emissions and transport and to forecast smoke particles and gaseous concentrations during the 2002 burning season in the South American and African continents. This system provides a useful tool for understanding the main atmospheric dynamic controls on the distribution and export of biomass burning emissions. Patterns and transient transport features which we discussed are reasonably described by the general understanding of the typical synoptic systems occurring in South America.

Comparisons between PM2.5 mass concentration measured at the surface and predicted by the numerical model show that this approach is able to capture the time variability of the smoke concentration; however, the comparison between the absolute values shows the model predictions systematically lower than the observations. Even higher emissions strengths might be indicated if this behavior is typical.

The disagreement regarding emissions may be due to several factors. One important factor is that there is a lack of information on the input parameters to the emission model. The biomass loading and the emission factors available in the literature were determined only for a few sites in South America and those numbers were scaled up using a vegetation map. This unavoidable procedure, with the dataset available to date, certainly is not consistent with the high heterogeneity of the Amazon biomes. Remote sensing of fires also has a number of difficulties. Cloud cover acts to reduce the number of fire pixels observed by the GOES WF_ABBA, along with other factors such as the size and intensity of the fire and satellite view angle. The ability of the GOES WF_ABBA to monitor fires every half hour is extremely helpful in being able to give the best opportunity to catch a glimpse of fire activity between the clouds. To date detailed studies to estimate the effect of cloud coverage on fire detection have not been performed. Since the GOES WF_ABBA fire product provides estimates of instantaneous fire size and not total burned area, comparisons with ground truth observations and estimates of fire size at the time of the GOES observation are difficult to determine. Comparisons with 3 fires during the SCAR-C and SCAR-B field programs indicated that the instantaneous GOES ABBA estimates were typically 20–50% greater than the estimated instantaneously observed fire size at a given time [5]. The fires in Brazil were from 8 to 25 acres in size. Considering a pixel size is over 2 orders of magnitude larger than this, it provides a much better estimate than simply assuming that the entire pixel is on fire. As for the number of fires detected by the GOES, recent ground truth studies in Acre have shown that throughout a day the GOES WF_ABBA observed roughly 70–80% of the fires that were identified on the ground [54]. Of course a fire may burn for a number of hours, but the GOES WF_ABBA may only be able to see it in one or two time periods due to cloud coverage or low intensity burning at the other time periods. Furthermore there is a distinct diurnal signature to the occurrence of anthropogenic fire activity in Brazil. The advantage of GOES is the ability to have numerous opportunities to detect a given fire throughout the day.

An alternative to this emission model would be the use of climatological biomass burning emission datasets [4, 52]. Model results using these cited datasets present more disagreements with observation, not only in the absolute values but also with regards to the time variability.

The Amazon basin does not have a dense meteorological observational network and this is reflected in the quality of the atmospheric analysis used as initial and boundary conditions for the atmospheric model integration. In addition, the presence of the smoke in the atmosphere results in strong radiative forcing as these particles are very efficient solar radiation scatterers and absorbers. The atmosphere responds to this forcing through a cooling of the low levels and a heating of the upper levels of the PBL. The net effect is an increase in the atmospheric thermodynamical stabilization. This will affect the aerosol vertical distribution by trapping the smoke, resulting in high concentrations near the ground where the observations were made. Ongoing model development includes coupling of this monitoring

system with an aerosol model which will be able to resolve the direct radiative effects of the smoke aerosol particles and improve the description of the boundary layer diurnal cycle. Finally, the model results represent an ensemble average in a 40 km grid cell while the observation is local and might not be representative of the model scale. Overall, the model is a powerful tool in understanding the synoptic controls on the biomass burning plume transport and has demonstrated good prediction skills.

Acknowledgements

This work was supported by Fundação de Amparo à Pesquisa do Estado de São Paulo (FAPESP), the Millennium Institute 'Global and Integrated Advancement of the Mathematics in Brazil' and Projects and Studies Financing Agency (FINEP), Brazil. A substantial part of the model development for this work was done by S. Freitas and R. Chatfield under a grant from US NASA's component of LBA-ECO, RTOP 622-94-13-10. The GOES WF_ABBA fire product was produced with funding from NOAA (NA07EC0676) and the NASA ESE IDS program. The views, opinions, and findings contained in this article are those of the author(s) and should not be construed as an official NOAA or US Government position, policy, or decision. The authors also thank Alexandre Correia and the anonymous reviewers for their very constructive comments.

References

1. Andreae, M.: 1991, Biomass burning: its history, use and distribution and its impact on environmental quality and global climate. In: J.S. Levine (ed.), *Global Biomass Burning: Atmospheric, Climatic and Biospheric Implications*, pp. 3–21, MIT Press, Cambridge, Mass.
2. Kaufman, Y.: 1995, Remote sensing of direct and indirect aerosol forcing. In: R.J. Charlson and J. Heintzenberg (eds.), *Aerosol Forcing of Climate*, pp. 297–332, John Wiley & Sons Ltd., Chichester.
3. Scholes, R., Ward, D. and Justice, C.: 1996, Emissions of trace gases and aerosols particles due to vegetation burning in southern hemisphere Africa, *J. Geophys. Res.* **101** (D19), 23667–23676.
4. Duncan, B., Martin, R., Staudt, A., Yevich, R. and Logan, J.: 2003, Interannual and seasonal variability of biomass burning emissions constrained by satellite observations, *J. Geophys. Res.* **108** (D2), 4100.
5. Prins, E., Feltz, J., Menzel, W. and Ward, D.: 1998, An overview of GOES-8 diurnal fire and smoke results for SCAR-B and 1995 fire season in South America, *J. Geophys. Res.* **103** (D24), 31821–31835.
6. Artaxo P., Gerab, F., Yamasoe, M. and Martins, J.: 1994, Fine mode aerosol composition in three long-term atmospheric monitoring sampling stations in the Amazon basin, *J. Geophys. Res.* **99**, 22857–22867.
7. Artaxo P., Fernandes, E., Martins, J. , Yamasoe, M., Hobbs, P., Maenhaut, W., Longo K. and Castanho, A.: 1998, Large-scale aerosol source apportionment in Amazonia, *J. Geophys. Res.* **103**, 31837–31847.

8. Echalar, F., Artaxo, P., Martins, J., Yamasoe M. and Gerab, F.: 1998, Long-term monitoring of atmospheric aerosols in the Amazon basin: Source identification and apportionment, *J. Geophys. Res.* **103**, 31849–31864.
9. Reid, J., Hobbs, P., Ferek, R., Blake, D., Martins, J., Dunlap, M. and Liousse, C.: 1998, Physical, chemical and optical properties of regional hazes dominated by smoke in Brazil, *J. Geophys. Res.* **103**, 32059–32080.
10. Jacobson, M.: 2001, Global direct radiative forcing due to multicomponent anthropogenic and natural aerosols, *J. Geophys. Res.* **106** (D2), 1551–1568.
11. Sato, M., Hansen, J., Koch, D., Lacis, A., Ruedy, R., Dubovik, O., Holben, B., Chin, M. and Novakov, T..: 2003, Global atmospheric black carbon inferred from AERONET, *Proc. Natl. Acad. Sci. USA*, **100**, 6319–6324.
12. Andreae, M.: 2001, The dark side of aerosols, *Nature*, **409**, 671–672.
13. Cotton, W. and Pielke, R.: 1996, *Human Impacts on Weather and Climate*, Cambridge University Press, New York.
14. Rosenfeld, D.: 1999, TRMM observed first direct evidence of smoke from forest fires inhibiting rainfall, *Geophys. Res. Lett.* **26**, 3101.
15. Grell, G., Emeis, S., Stockwell, W., Schoenemeyer, T., Forkel, R., Michalakes, J., Knoche, R. and Seidl, W.: 2000, Application of a multiscale, coupled MM5/chemistry model to the complex terrain of the VOTALP valley campaign, *Atmos. Env.* **34**, 1435–1453.
16. Chatfield, R., Vastano, J., Singh, H. and Sachse, G.: 1996, A general model of how fire emissions and chemistry produce African/oceanic plumes (O3, CO, PAN, smoke), *J. Geophys. Res.* **101** (D19), 24279–24306.
17. Chatfield, R., Guo, Z., Sachse, G., Blake, D. and Blake, N.: 2002, The subtropical global plume in the Pacific Exploratory Mission-Tropics A (PEM-Tropics A), PEM-Tropics B and the Global Atmospheric Sampling Program (GASP): How tropical emissions affect the remote Pacific. *J. Geophys. Res.*, **107** (D16), 4278.
18. Chin, M., Rood, R., Lin, S.-J., Muller, J.-F. and Thompson, A.: 2000, Atmospheric sulfur cycle simulated in the global model GOCART: Model description and global properties, *J. Geophys. Res.* **105** (D20), 24671–24687.
19. Brasseur, G., Hauglustaine, D., Walters, S., Rasch, P., Müller, J.-F., Granier, C. and Tie, X.: 1998, MOZART, a global chemical transport model for ozone and related chemical tracers, 1: Model description, *J. Geophys. Res.* **103** (D21), 28265–28289.
20. Horowitz, L., Walters, S., Mauzerall, D., Emmons, L., Rasch, P., Granier, C., Tie, X., Lamarque, J.-F., Schultz, M. and Brasseur, G.: 2003, A global simulation of tropospheric ozone and related tracers: Description and evaluation of MOZART, version 2, *J. Geophys. Res.* **108** (D24), 4784.
21. Walko, R., Band, L., Baron J., Kittel, F., Lammers, R., Lee, T., Ojima, D., Pielke, R., Taylor, C., Tague, C., Tremback, C. and Vidale, P.: 2000, Coupled atmosphere-biophysics-hydrology models for environmental modeling, *J. Appl. Meteorol.* **39**, 931–944.
22. Lobert, J.M. and Warnatz, J.: 1993, Emissions from the combustion process in vegetation. In: P.J. Crutzen and J. Goldamner (eds.), *Fire in the Environment: Its Ecological, Atmospheric and Climatic Importance*, pp. 15–38, John Wiley & Sons Ltd., Chichester.
23. Ward, E., Susott, R., Kaufman, J., Babbit, R., Cummings, D., Dias, B., Holben, B., Kaufman, Y., Rasmussen, R. and Setzer, A.: 1992, Smoke and fire characteristics for cerrado and deforestation burns in Brazil: BASE-B Experiment, *J. Geophys. Res.* **97** (D13), 14601–14619.
24. Ferek, J., Reid, J. and Hobbs, P.: 1996, Emission factors of hydrocarbons, halocarbons, trace gases and particles from biomass burning in Brazil. In: V. Kirchhoff (ed.), *Smoke/Sulfate, Clouds and Radiation – Brazil (SCAR-B) Proceedings*, pp. 35–39, Transtec Editorial, Fortaleza.
25. Andreae, M. and Merlet, P.: 2001, Emission of trace gases and aerosols from biomass burning, *Global Biogeochem. Cycles*, **15**, 955–966.
26. Pereira, M.: 1988, *Detecção, Monitoramento e Análises de alguns Impactos Ambientais de Queimadas na Amazônia Usando Dados de Avião e dos Satélites NOAA e LANDSAT.* Disser-

tação de mestrado, INPE-4503-TDL/326, 268 p., Instituto Nacional de Pesquisas Espaciais (in Portuguese).
27. Setzer, A. and Pereira, M.: 1991, Amazonia biomass burnings in 1987 and an estimate of their tropospheric emissions, *Ambio*, **20**, 19–22.
28. Prins, E. and Menzel, W.: 1992, Geostationary satellite detection of biomass burning in South America, *Int. J. Remote Sens.*, **13**, 2783–2799.
29. Matson, M. and Dozier, J.: 1981, Identification of sub-resolution high temperature sources using a thermal IR sensor, *Photogram. Eng. Remote Sens.*, **47**, 1311–1318.
30. Prins, E., Menzel, W. and Ward, D.: 1996, GOES-8 ABBA diurnal fire monitoring during SCAR-B. In: V. Kirchhoff (ed.), *Smoke/Sulfate, Clouds and Radiation – Brazil (SCAR-B) Proceedings*, pp. 153–157, Transtec Editorial, Fortaleza.
31. Chatfield, R. and Crutzen, P.: 1984, Sulfur dioxide in remote oceanic air: Cloud transport of reactive precursors, *J. Geophys. Res.*, **89** (D5), 7111–7132.
32. Pickering, K., Dickerson, R., Huffman, G., Boatman. J. and Schanot, A.: 1988, Trace gas transport in the vicinity of frontal convective clouds, *J. Geophys. Res.* **93** (D1), 759–773.
33. Chatfield, R. and Delany, A.: 1990, Convection links biomass burning to increased tropical ozone: However, models will tend to overpredict O3, *J. Geophys. Res.* **95** (D12), 18473–18488.
34. Thompson, A., Pickering, K., Dickerson, R., Ellis, Jr. W., Jacob, D., Scala, J., Tao, W.-K., McNamara, D. and Simpson, J.: 1994, Convective transport over the Central United States and its role in regional CO and ozone budgets, *J. Geophys. Res.* **99** (D09), 18703–18711.
35. Freitas, S., Silva Dias, M., Silva Dias, P., Longo, K., Artaxo, P., Andreae, M. and Fischer, H.: 2000, A convective kinematic trajectory technique for low-resolution atmospheric models, *J. Geophys. Res.* **105** (D19), 24375–24386.
36. Longo, K., Thompson, A., Kirchhoff, V., Remer, L., Freitas S., Silva Dias, M., Artaxo, P., Hart, W., Spinhirne, J. and Yamasoe, M.: 1999, Correlation between smoke and tropospheric ozone concentration in Cuiabá during Smoke, Clouds and Radiation-Brazil (SCAR-B), *J. Geophys. Res.* **104** (D10), 12113.
37. Freitas, S., Silva Dias, M. and Silva Dias, P.: 2000, Modeling the convective transport of trace gases by deep and moist convection*, Hybrid Meth. Eng.*, **2** (3), 317–330.
38. Galanter, M., Levy, II H. and Carmichael, G.: 2000, Impacts of biomass burning on tropospheric CO, NOx, and O3, *J. Geophys. Res.* **105** (D5), 6633–6653.
39. Andreae, M., Artaxo, P., Fischer, H., Freitas, S., Grégoire, J.-M., Hansel, A., Hoor, P., Kormann, R., Krejci, R., Lange, L., Lelieveld, J., Lindinger, W., Longo, K., Peters, W., Reus, M., Scheeren, B., Silva Dias, M. A. F., Ström, J., Velthoven, P. F. J. and Williams, J.: 2001, Transport of biomass burning smoke to the upper troposphere by deep convection in the equatorial region, *Geophys. Res. Lett.* **28** (6), 951.
40. Tripoli, G. and Cotton, W.: 1982, The Colorado State University three-dimensional cloud/mesoscale model. Part I: General theoretical framework and sensitivity experiments, *J. Res. Atmos.* **16**, 185–219.
41. Tremback, C.: 1990, *Numerical Simulation of a Mesoscale Convective Complex: Model Development and Numerical Results.* Ph.D. Dissertation, Atmos. Sci. Paper No. 465, Colorado State University, Dept. of Atmospheric Science, Fort Collins, CO.
42. Grell, G.: 1993, Prognostic evaluation of assumptions used by cumulus parameterization, *Mon. Wea. Rev.* **121** 764–787.
43. Grell, G. and Devenyi, D.: 2002, A generalized approach to parameterizing convection combining ensemble and data assimilation techniques, *Geophys. Res. Lett.* **29**, 1693.
44. Belward, A.: 1996, The IGBP-DIS global 1 km land cover data set (DISCover)-proposal and implementation plans, IGBP-DIS Working Paper No. 13, Toulouse, France.
45. Seinfeld, J. and Pandis, S.: 1998, *Atmospheric Chemistry and Physics*, John Wiley & Sons Inc., New York.

46. Mauzerall, D., Logan, J., Jacob, D., Anderson, B., Blake, D., Bradshaw, J., Heikes, B., Sachse, G., Singh, H. and Talbot, B.: 1998, Photochemistry in biomass burning plumes and implications for tropospheric ozone over the tropical South Atlantic, *J. Geophys. Res.* **103** (D7), 8401–8423.
47. Berge, E.: 1993, Coupling of wet scavenging of sulphur to clouds in a numerical weather prediction model, *Tellus* **45B**, 1–22.
48. Chuang, C., Penner, J. and Edwards, L.: 1992, Nucleation scavenging of smoke particles and simulated drop size distributions over large biomass fires, *J. Atmos. Sci.* **14**, 1264–1275.
49. Smagorinsky, J.: 1963, General circulation experiments with the primitive equations. Part I: The basic experiment, *Mon. Wea. Rev.* **91**, 99–164.
50. Mellor, G. and Yamada, T.: 1974, A hierarchy of turbulence closure models for planetary boundary layers, *J. Atmos. Sci.* **31**, 1791–1806.
51. Tremback, C., Powell, J., Cotton, W. and Pielke, R.: 1987, The forward in time upstream advection scheme: Extension to higher orders, *Mon. Wea. Rev.* **115**, 540–555.
52. Olivier, J., Bouwman, A., van der Maas, C., Berdowski, J., Veldt, C., Bloos, J., Visschedijk, A., Zandveld, P. and Haverlag, J.: 1996, *Description of EDGAR Version 2.0: A Set of Global Emission Inventories of Greenhouse Gases and Ozone-Depleting Substances for All Anthropogenic and Most Natural Sources on a per Country Basis and on a 1x1 Degree Grid*, RIVM Report 771060 002/TNO-MEP Report R96/119, National Institute of Public Health and the Environment, Bilthoven, the Netherlands.
53. Satyamurty, P., Nobre, C. and Silva Dias, P.: 1998, South America. In: D. Karoly and Vincent D., (eds.), *Meteorology of the Southern Hemisphere,* Meteorological Monographs **27** No. 49, pp. 119–139, American Meteorological Society, Boston.
54. McClaid-Cook, K., Selhorst, D., Widson, J., Pantoja, N., Brown, I., Prins, E., Feltz, J. and Fonseca Duarte, A. A.: 2003, Estimation of Amazon biomass burning events in Acre, Brazil using GOES-8 and AVHRR hot pixel data. In: *The 99th Annual Meeting of the Association of American Geographers*, New Orleans, Lousiania, March 5–8.